ORGANOMETALLICS
Article

Organometallics **2009,** *28,* 3691–3699 3691
DOI: 10.1021/om900107y

Rigid Bis(tetrathiafulvalenes) Doubly Bridged by Phosphino Groups and Derivatives: Synthesis and Intramolecular Mixed Valence State

Ion Danila,[†] Frédéric Biaso,[‡] Helena Sidorenkova,[‡] Michel Geoffroy,*[,‡] Marc Fourmigué,[§] E. Levillain,[†] and Narcis Avarvari*[,†]

[†]*Laboratoire Chimie et Ingénierie Moléculaire (CIMA), UMR 6200 CNRS−Université d'Angers, UFR Sciences, Bâtiment K, 2 Boulevard Lavoisier, 49045 Angers, France,* [‡]*Department of Physical Chemistry, University of Geneva, 30 Quai Ernest Ansermet, 1211 Geneva, Switzerland, and* [§]*Sciences Chimiques de Rennes, UMR 6226 CNRS−Université Rennes I, Campus de Beaulieu, 35042 Rennes, France*

Received February 11, 2009

The synthesis and structural characterization of the λ^5-bis(phosphine sulfide) and the bimetallic complexes bis[phosphino-$M(CO)_5$] (M = Mo, W) of the 3,4-dimethyltetrathiafulvalene (*ortho*-DMTTF)-based rigid dimer $(PPh)_2$(*o*-DMTTF)$_2$, containing a central 1,4-dihydro-1,4-diphosphinine ring, are described. Single-crystal X-ray analyses have been performed for the *trans* isomers $(PhPX)_2$(*o*-DMTTF)$_2$ (X = S, $Mo(CO)_5$, and $W(CO)_5$) and for the *cis* isomer $[PhPW(CO)_5]_2$-(*o*-DMTTF)$_2$. Planar or slightly folded boat-type conformations are observed for the central six-membered ring, together with different packings characterized by short intermolecular S···S contacts. The optical signature of the oxidized species in the case of the free ligand $(PPh)_2$-(*o*-DMTTF)$_2$ has been evidenced by UV−vis spectroelectrochemistry measurements. Solution EPR measurements on the radical cation species of $(PPh)_2$(*o*-DMTTF)$_2$ definitely assess the full delocalization of the unpaired electron over both electroactive TTF units, with an associated coupling of 0.48 G with 12 equivalent protons. The EPR signal of the dication proves the radical nature of this species, in favor of a triplet ground state. The radical cation of the *cis*-$[PhPW(CO)_5]_2$-(*o*-DMTTF)$_2$ isomer was also investigated by EPR, for which the observed hyperfine structure demonstrates the extended delocalization of the electron, together with a larger coupling constant with the phosphorus nuclei. DFT calculations for the radical cation of $(PPh)_2$(*o*-DMTTF)$_2$ afford a boat-type conformation for the central ring and a SOMO consistent with a full delocalization of the electron over both TTF units. Moreover, the calculations indicate that in the case of the dication of $(PPh)_2$(*o*-DMTTF)$_2$ the triplet state is more stable by 11.7 kcal mol^{-1} than the singlet state.

Introduction

One of the most valuable strategies to achieve mixed valence states in a controlled manner in the field of tetrathiafulvalenes (TTF),[1] which represent a well-known class of sulfur-rich organic electron donors extensively investigated as precursors for molecular metals and superconductors,[2] consists in the use of dimeric TTFs.[3] Indeed, in such compounds, through-bond or through-space interactions can promote electronic communication between the redox-active units, depending on the nature of the linkage between the TTFs, and thus eventually allowing for the observation and isolation, in either solution or solid state, of intramolecular mixed valence species. In the corresponding crystalline radical cation salts or charge transfer complexes of bis(TTFs), enhanced dimensionality, due to weaker intersite electrostatic repulsions and more numerous S···S contacts, might be observed, providing original architectures and unusual band structures.[4] Besides the direct linking of TTF units through a single C−C bond,[3a,5] a valuable strategy to connect two TTFs in close vicinity consists in the utilization of monatomic based linkers, thus allowing access to the

*Corresponding authors. (M.G.) E-mail: Michel.Geoffroy@chiphy.unige.ch. (N.A.) Fax: (+33)02 41 73 54 05. E-mail: narcis.avarvari@univ-angers.fr.

(1) (a) Segura, J. L.; Martin, N. *Angew. Chem., Int. Ed.* **2001**, *40*, 1372. (b) Yamada, J.-L. *TTF Chemistry: Fundamentals and Applications of Tetrathiafulvalene*; Springer-Verlag: Berlin, 2004.

(2) (a) Williams, J. M.; Ferraro, J. R.; Thorn, R. J.; Carlson, K. D.; Geiser, U.; Wang, H. H.; Kini, A. M.; Whangbo, M.-H. *Organic Superconductors (Including Fullerenes), Synthesis, Structure, Properties and Theory*; Grimes, R. N., Ed.; Prentice-Hall: Englewoods Cliffs, NJ, 1992. (b) Ishiguro, T.; Yamaji, K.; Saito, G. Organic Superconductors; Springer-Verlag, Heidelberg, 1998.

(3) (a) Becker, J. Y.; Bernstein, J.; Ellern, A.; Gershtenman, H.; Khodorkovsky, V. *J. Mater. Chem.* **1995**, *5*, 1557. (b) Otsubo, T.; Aso, Y.; Takimiya, K. *Adv. Mater.* **1996**, *8*, 203. (c) Iyoda, M.; Hasegawa, M.; Miyake, Y. *Chem. Rev.* **2004**, *104*, 5085.

(4) (a) Bryce, M. R. *J. Mater. Chem.* **1995**, *5*, 1481. (b) Mézière, C.; Fourmigué, M.; Canadell, E.; Clérac, R.; Bechgaard, K.; Auban-Senzier, P. *Chem. Mater.* **2000**, *12*, 2250. (c) Garcia-Yoldi, I.; Miller, J. S.; Novoa, J. J. *J. Phys. Chem. A* **2009**, *113*, 484.

(5) (a) Iyoda, M.; Ogura, E.; Hara, K.; Kuwatani, Y.; Nishikawa, H.; Sato, T.; Kikuchi, K.; Ikemoto, I.; Mori, T. *J. Mater. Chem.* **1999**, *9*, 335. (b) John, D. E.; Moore, A. J.; Bryce, M. R.; Batsanov, A. S.; Leech, M. A.; Howard, J. A. K. *J. Mater. Chem.* **2000**, *10*, 1273. (c) Iyoda, M.; Hara, K.; Kuwatani, Y.; Nagase, S. *Org. Lett.* **2000**, *2*, 2217. (d) Kageyama, T.; Ueno, S.; Takimiya, K.; Aso, Y.; Otsubo, T. *Eur. J. Org. Chem.* **2001**, 2983. (e) Iyoda, M.; Hara, K.; Ogura, E.; Takano, T.; Hasegawa, M.; Yoshida, M.; Kuwatani, Y.; Nishikawa, H.; Kikuchi, K.; Ikemoto, I.; Mori, T. *J. Solid State Chem.* **2002**, *168*, 597.

Published on Web 06/15/2009

general series formulated as $X(TTF)_2$, with X = S or Se,[6] Te,[7] PPh, $SiMe_2$ or Hg,[8] and SbMe,[9] where TTF is the parent compound or substituted derivatives. However, these compounds are inherently flexible, since it exists *a priori* the possibility of free rotation to occur around the C−X simple bonds and, hence, a decrease of the conjugation between the redox-active sites through the spacer. Therefore, in order to overcome this structural flexibility, more rigid derivatives have been synthesized, upon attachment of the TTF units by a second bridge. Accordingly, in the compounds $X_2(TTF)_2$ (X = S[10] or Te[11]), the TTF units are connected through two linkers, giving rise to a central six-membered ring, which can be more or less distorted.

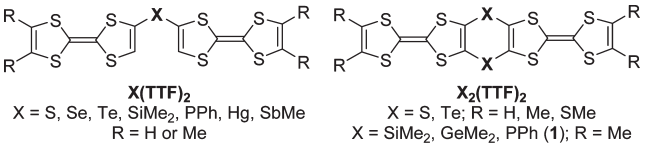

Note that analogous selenium-based donors have been obtained by the use of two methyl-antimony (SbMe) linkers between two tetraselenafulvalene (TSF) units.[9]

In this respect, we have recently described rigid bis(*o*-DMTTFs) (*o*-DMTTF = *ortho*-dimethyltetrathiafulvalene), in which the linkers were either $SiMe_2$ and $GeMe_2$ fragments[12] or phenylphosphino (PPh) groups.[13] In the silicon- and germanium-based dimers we have proved the extended electron delocalization in the radical cation state, through theoretical calculations and experimental investigations, such as EPR spectroscopy, and have isolated the corresponding mixed valence species in the solid state. On the other hand, even though the *cis* isomer of the redox-active 1,4-diphosphinine *cis*-$(PPh)_2$(*o*-DMTTF)$_2$ (*cis*-**1**) shows in solution sequential one-electron oxidation into radical cation and then dication species, its electrocrystallization provided a charge-localized crystalline salt with the $[Mo_6O_{19}]^{2-}$ anion, in which one TTF unit was oxidized into radical cation while the other TTF of the dimer was essentially neutral. Moreover, the phosphorus atoms were found to be oxidized into phosphine oxide.[13] It is obvious that one of the main interests related to the compound **1**, which can exist as a *cis* or *trans* isomer, is related to the reactivity and the coordination properties of the phosphorus atoms. Indeed, one might envisage the preparation of λ^5-P derivatives or bimetallic complexes in which the electronic properties of the redox-active units are expected to vary with respect to those of the free ligand **1**. We report herein the synthesis and structural characterization of the bis(P-sulfide) derivative of **1**, along with bimetallic complexes based on the pentacarbonyl fragments $W(CO)_5$ and $Mo(CO)_5$. Furthermore, the intramolecular electronic communication between the TTF units in **1** and its derivatives is investigated through solution EPR measurements and theoretical calculations.

Scheme 1. Reactivity of 1

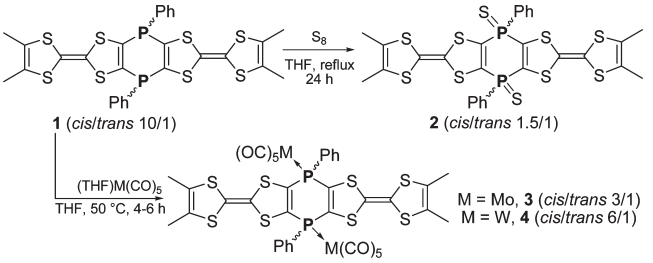

Results and Discussion

Synthesis and Crystal Structures. The synthesis of $(PhP)_2$(*o*-DMTTF)$_2$, **1**, as a mixture of *cis* (major, ∼90%) and *trans* (minor, ∼10%) isomers, upon lithiation and subsequent trapping with $PhPCl_2$ has been previously described.[13] In the course of our experiments we noticed that solutions in THF or toluene of pure *cis*-**1** were slowly evolving upon moderate heating at 70 °C toward enrichment in *trans*-**1**. This behavior is very likely related to the pyramidal inversion of the phosphines,[14] for which the energy barrier is generally lower when the phosphorus atom bears aromatic rings and/or unsaturated substituents such as vinyl or ethynyl groups and can be observed also in the case of cyclic phosphines.[15] The rationale for the weaker inversion barrier can be explained on the basis of the stabilization of the planar transition state provided by the overlap between the lone pairs of the phosphorus atoms and the π vinylic orbitals. Since the reactions we envisaged were expected to occur upon thermal activation, we decided to investigate the reactivity of the *cis*/*trans* mixture of **1** and then to eventually proceed to the separation of the two isomers. The reaction of **1** with a large excess of sulfur under reflux of THF during 24 h provides a mixture of phosphine sulfides *cis*-**2** and *trans*-**2** in a ratio of 1.5:1, which is very difficult to separate by column chromatography (Scheme 1). The progress of the reaction was followed by ^{31}P NMR spectroscopy, which indicates a deshielding of the phosphorus atom resonances when compared to those of *cis*/*trans* **1**. Indeed, two close singlets are now observed at +11.6 ppm (*cis*) and +12.0 ppm (*trans*), while in the starting ligand **1** the singlets corresponding to the *cis* and *trans* isomers appear at −21.5 and −25.6 ppm, respectively. The composition of the reaction product mixture, in which the proportion of *trans*-**2** with respect to *trans*-**1** in the starting free phosphine is much larger, demonstrates that the use of pure *cis*-**1** or *trans*-**1** in the sulfuration reaction is not justified, since an inversion process occurs under these conditions. Only fractions in which one or the other isomer were dominant could be obtained after chromatographic workup, yet slow evaporation of a CH_2Cl_2 solution enriched in *trans*-**2** afforded single crystals of this isomer.

(6) Bryce, M. R.; Cooke, G.; Dhindsa, A. S.; Ando, D. J.; Hursthouse, M. B. *Tetrahedron Lett*. **1992**, *33*, 1783.
(7) (a) Becker, J. Y.; Bernstein, J.; Dayan, M.; Shahal, L. *J. Chem. Soc., Chem. Commun*. **1992**, 1048. (b) Martin, J. D.; Canadell, E.; Becker, J. Y.; Bernstein, J. *Chem. Mater*. **1993**, *5*, 1199.
(8) Fourmigué, M.; Huang, Y.-S. *Organometallics* **1993**, *12*, 797.
(9) Ashizawa, M.; Yamamoto, H. M.; Nakao, A.; Kato, R. *Tetrahedron Lett*. **2006**, *47*, 8937.
(10) (a) Khodorkovsky, V. Y.; Becker, J. Y.; Bernstein, J. *Synth. Met*. **1993**, *56*, 1931. (b) Aqad, E.; Becker, J. Y.; Bernstein, J.; Ellern, A.; Khodorkovsky, V.; Shapiro, L. *J. Chem. Soc., Chem. Commun*. **1994**, 2775.
(11) (a) Wang, C.; Ellern, A.; Becker, J. Y.; Bernstein, J. *Tetrahedron Lett*. **1994**, *35*, 8489. (b) Wang, C.; Ellern, A.; Khodorkovsky, V.; Becker, J. Y.; Bernstein, J. *J. Chem. Soc., Chem. Commun*. **1994**, 2115. (c) Ojima, E.; Fujiwara, H.; Kobayashi, H.; Kobayashi, A. *Adv. Mater*. **1999**, *11*, 1527.
(12) Biaso, F.; Geoffroy, M.; Canadell, E.; Auban-Senzier, P.; Levillain, E.; Fourmigué, M.; Avarvari, N. *Chem.—Eur. J*. **2007**, *13*, 5394.
(13) Avarvari, N.; Fourmigué, M. *Chem. Commun*. **2004**, 2794.
(14) Baechler, R. D.; Mislow, K. *J. Am. Chem. Soc*. **1970**, *92*, 3090.
(15) Märkl, G.; Zollitsch, T.; Kreitmeier, P.; Prinzhorn, M.; Reithinger, S.; Eibler, E. *Chem.—Eur. J*. **2000**, *6*, 3806.

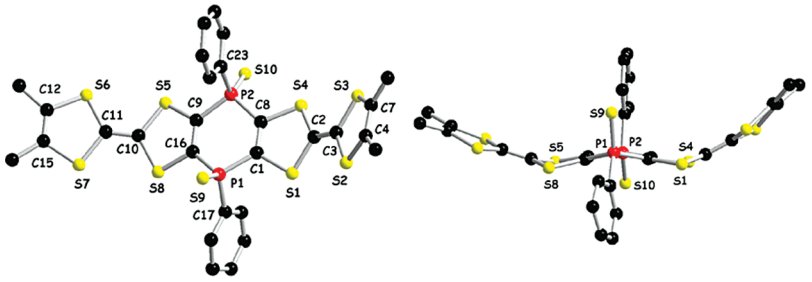

Figure 1. View of *trans*-**2** (H atoms omitted) (left) and side view of the molecule (right).

Table 1. Bond Distances and Folding Angles in the Compounds 2−4

	trans-**2**·H_2O	*trans*-**3**·C_7H_8	*cis*-**4**·CH_2Cl_2	*trans*-**4**·C_7H_8
		Average Bond Distances (Å)		
P−M or P−S	1.940(3)	2.500(13)	2.482(2)	2.494(1)
M−C(CO) axial		2.014(7)	1.999(10)	2.017(5)
M−C(CO) equatorial		2.046(7)	2.043(10)	2.044(6)
C═O axial		1.132(8)	1.160(10)	1.137(6)
C═O equatorial		1.132(7)	1.146(10)	1.134(6)
central C═C of the TTF	1.342(8)	1.344(7)	1.344(9)	1.341(6)
diphosphinine C═C	1.331(8)	1.338(6)	1.341(9)	1.339(7)
		Folding Angles (deg)		
along S···S axis, internal cycle	27.5(3)	20.4(3)	19.8(3)	17.6(3)
	30.9(2)	11.8(3)	17.3(3)	
along P···P axis	18.6(1)	0.0	14.5(4)	0.0
deviation of the P atoms from the mean plane of the four C atoms of the central ring (Å)	0.122(2) 0.335(1) (same molecule)	0.0 0.076(1) (two molecules)	0.208(2) 0.154(2) (same molecule)	0.289(8)

The bis(phosphine sulfide) *trans*-**2** crystallizes in the monoclinic system, space group $C2/c$, with one independent molecule in the asymmetric unit. Note the presence of a crystallization water molecule, very likely the consequence of the aerial evaporation process during which no special conditions have been taken. The relative *trans* configuration of the phenyl and sulfur substituents on the P atoms with respect to the central six-membered ring was undoubtedly established, thus allowing also the assignment of the ^{31}P NMR resonances of the two isomers (Figure 1).

Selected bond lengths and angles are given in Table 1. The C(2)═C(3) and C(10)═C(11) bonds (average 1.342 Å), as well as C(1)═C(8) and C(9)═C(16) (average 1.331 Å) of the central six-membered ring, are comparable with those in *cis*-**1** and lie in the typical range for neutral TTFs. It is worthwhile noting the boat-like conformation of the 1,4-diphosphinine cycle, with a folding angle of 18.6(1)°, which is much smaller than the one observed in *cis*-**1** (30.4(1)°). Both TTFs units are strongly folded around the S(1)···S(4) (30.9(2)°) and S(5)···S(8) (27.5(3)°) axes. The donors stack along the *c* direction (see Supporting Information), with the establishment of several intermolecular S···S contacts below 4.0 Å, among which the shortest one, of 3.69 Å, corresponds to a P═S···S═P interaction.

The bimetallic complexes **3** (Mo) and **4** (W) have been conventionally synthesized upon thermal displacement of the THF ligand from the starting complexes (THF)$M(CO)_5$ by the phosphine. Longer heating periods were necessary in the case of the Mo-based complex, less reactive than the W counterpart; therefore in the final reaction mixtures the ratio *cis*/*trans* was different, as assessed by ^{31}P NMR spectroscopy. Note the stronger downfield shift in ^{31}P resonances in the case of the Mo complexes, appearing at +18.9 (*cis*) and +20.0 ppm (*trans*), when compared to the W ones, at +0.9 (*cis*) and +0.4 ppm (*trans*), a feature already observed in the mononuclear diphosphine $[(CO)_4M(PPh_2)_2]$(*o*-DMTTF) (M = Mo, W) complexes.[16] The *cis*/*trans* mixture of $[(CO)_5Mo(PPh)]_2$(*o*-DMTTF)$_2$ (**3**) could not be separated by column chromatography, unlike the complexes $[(CO)_5W(PPh)]_2$(*o*-DMTTF)$_2$, **4**, for which an efficient separation of the *cis* and *trans* isomers could be achieved. However, recrystallization of *cis*/*trans* **3** from toluene afforded two types of crystals, which were eventually manually separated. Only the *trans*-**3** crystals proved to be suitable for X-ray diffraction analysis on single crystals. The complex crystallizes in the triclinic system, space group $P\bar{1}$ (Table 2), with two independent half-molecules, both located on inversion centers, in the asymmetric unit, which further contains one-half of a crystallization toluene molecule disordered about the inversion center. The two molecules of bimetallic complexes **A** and **B** differ essentially only by the folding angle along the internal S···S hinge, which amounts to 11.8° for **A** and 20.4° for **B**, while the central six-membered ring is perfectly planar for both of them (Figure 2).

The complexes **A** and **B** stack alternatively along *c*, with the setting of intermolecular S···S contacts of 4.0 Å between molecules belonging to neighboring columns, while within the same column the S···S distances are much longer (Figure 3). It is thus clear that the system, despite the

(16) Avarvari, N.; Martin, D.; Fourmigué, M. *J. Organomet. Chem.* **2002**, *643−644*, 292.

Table 2. Crystallographic Data, Details of Data Collection, and Structure Refinement Parameters

	trans-**2**·H_2O	*trans*-**3**·C_7H_8	*cis*-**4**·CH_2Cl_2	*trans*-**4**·C_7H_8
formula	$C_{28}H_{22}O_2P_2S_{10}$	$C_{48.5}H_{34}Mo_2O_{10}P_2S_8$	$C_{38.5}H_{22}Cl_2P_2O_{10}S_8W_2$	$C_{52}H_{38}P_2O_{10}S_8W_2$
MW	773.00	1317.07	1373.14	1508.94
cryst syst	monoclinic	triclinic	triclinic	monoclinic
space group	$C2/c$	$P\bar{1}$	$P\bar{1}$	$P2_1/c$
a (Å)	46.8281(9)	12.408 (2)	12.237(2)	14.098(3)
b (Å)	10.7262(11)	13.205(1)	13.939(3)	12.607(3)
c (Å)	15.665(3)	9.364(1)	14.864(3)	15.831(3)
α (deg)	90	96.91(1)	106.82(3)	90
β (deg)	107.501(8)	104.46(1)	105.47(3)	100.44(3)
γ (deg)	90	111.17(1)	92.66(3)	90
V (Å^3)	7503.9(16)	2786.00(44)	2317.90(34)	2767.12(15)
Z	8	2	2	2
d_{calcd} (g cm^{-3})	1.368	1.570	1.967	1.811
μ (mm^{-1})	0.697	0.864	5.499	4.570
T (K)	293(2)	293(2)	293(2)	293(2)
λ (Å)	0.71073	0.71073	0.71073	0.71073
$R(F_o)^a$	0.068	0.052	0.037	0.030
$R_w(F_o^2)^a$	0.214	0.152	0.056	0.067

^{a} $R(F_o) = \sum||F_o| - |F_c||/\sum|F_o|$; $R_w(F_o^2) = [\sum[w(F_o^2 - F_c^2)^2]/\sum[w(F_o^2)^2]]^{1/2}$.

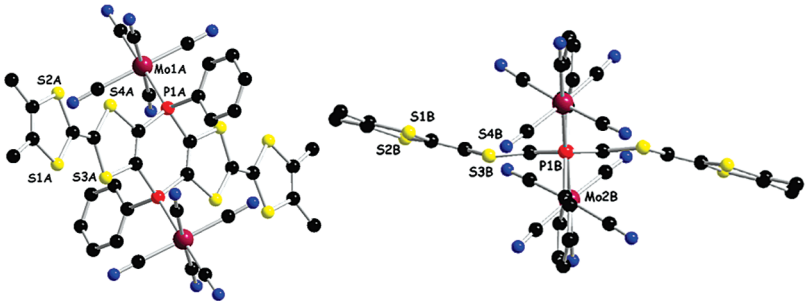

Figure 2. View of *trans*-**3** molecule **A** (left) and side view of the molecule **B** (right) showing the planar conformation of the central ring (H atoms omitted).

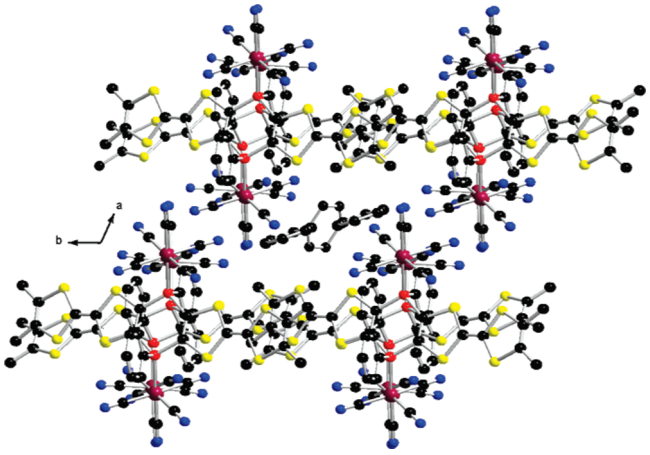

Figure 3. Packing diagram of *trans*-**3** in the plane *ab*. The shortest S···S intermolecular interactions are established between donors of parallel columns along *c*.

important steric hindrance provided by the aromatic rings and organometallic fragments, still accommodates intermolecular short interactions between the redox-active units.

Interestingly, the tungsten bimetallic complexes *cis*-**4** and *trans*-**4** have different elution behavior, and thus they were readily separated by column chromatography. Moreover, suitable single crystals for X-ray analysis could be grown for both isomers. Although the crystallization conditions were basically the same, *trans*-**3** and *trans*-**4** are not isostructural.

As expected, both *cis*-**4** and *trans*-**4** structures show octahedral coordination geometry around the tungsten center, as in the case of the molybdenum counterpart, with bond lengths and angles in the normal range. The *cis* isomer crystallizes in the triclinic system, space group $P\bar{1}$, with one independent molecule in the asymmetric unit in general position, while the *trans* one crystallizes in the monoclinic system, space group $P2_1/c$, with one independent half-molecule in the asymmetric unit (Table 2). Both crystals contain solvent molecules, i.e., methylene chloride in *cis*-**4** and toluene in *trans*-**4**. The 1,4-dihydrodiphosphinine ring in the *cis* complex is less distorted than in the free ligand, with the corresponding dihedral angle along the P(1)···P(2) hinge amounting now to 14.5(4)°, within a boat conformation (Figure 4). On the other hand, the *trans* isomer crystallizes in a chairlike conformation, more pronounced than in *trans*-**3**, with an essentially planar 1,4-dihydro-1,4-diphosphinine ring, in which the P atoms lie 0.289(8) Å above and below the plane defined by the four carbon atoms of the six-membered ring (Figure 4).

Intermolecular S···S distances amounting to 3.89−3.92 Å are established in the structure of *cis*-**4** through stacking of molecules belonging to two parallel columns (Figure 5), while these contacts are much longer (4.48 Å) in the case of *trans*-**4** (Supporting Information).

It is interesting to note once again that the rigid bis(TTFs) can accommodate rather short S···S contacts thanks to the length of the molecule overcoming the central steric hindrance due to the metal−carbonyl fragments and the phenyl rings. Note that these latter engage in $\pi-\pi$ intermolecular interactions.

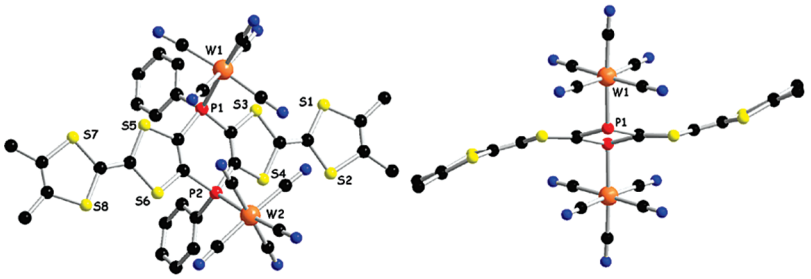

Figure 4. Molecular structure of *cis*-**4** (left) and side view of *trans*-**4** (right) showing the distortion of the central ring (H atoms omitted, Ph groups omitted in *trans*-**4**).

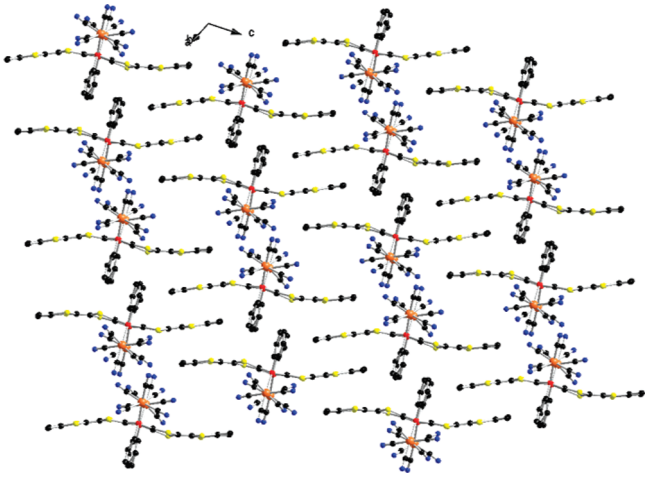

Figure 5. Packing diagram of *cis*-**4**. Voids between TTF fragments along the stacking direction are filled with solvent molecules (H atoms and solvent omitted).

Electrochemical Studies. As previously described,[13] cyclic voltammetry measurements performed on the *cis*-**1** ligand show splitting of both oxidation waves, consistent with the stepwise formation of the radical cation, dication, trication, and tetracation species upon reversible one-electron oxidation processes. The potential difference ΔE amounts to 120 mV between the first two oxidation peaks and also between the oxidation processes three and four. In order to get more insight into the formation of the oxidized species of *cis*-**1**, we have first carried out UV−vis spectroelectrochemistry measurements.

Thin-layer cyclic voltammetry measurements (TLCV) revealed that both the first and second pair of oxidation waves correspond to two one-electron processes (see Experimental Section). At potentials below 0.4 V one can observe only the typical optical signature of a neutral TTF, with a λ_{max} at 338 nm (Figure 6 and Supporting Information).[17] Then, once the radical cation is generated, two new absorption bands centered at λ_{max} 463 and 652 nm appear, with concomitant disappearance of the band at 338 nm. These two main absorptions are typical for TTF radical cation species and have been assigned in the case of the simple $TTF^{+\bullet}$ radical cation to a HOMO−1 → SOMO transition for the less energetic one and a SOMO → π^* transition for the most

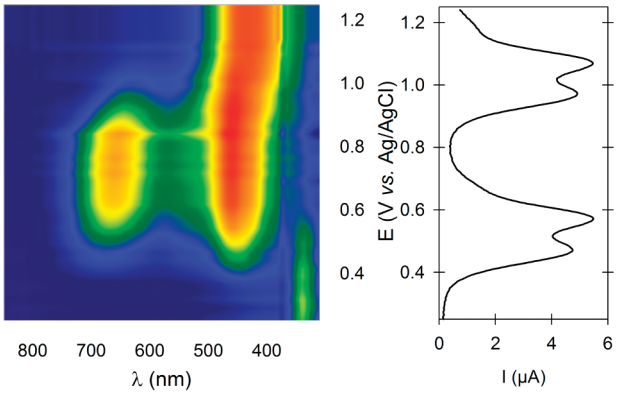

Figure 6. UV−vis spectroelectrochemistry of *cis*-**1**.

intense one, occurring at lower wavelength.[18] Note that these bands in our case are red-shifted with respect to those of the parent TTF, and they compare very well with the experimental values measured for the radical cation of the tetramethyltetrathiafulvalene (TMTTF).[17a,19] Upon increasing the potential up to 0.8 V, where very likely only the dicationic $[cis\text{-}\mathbf{1}]^{2+}$ species is present, there is no noticeable difference in the position of the bands between the mono- and the dication. This suggests that the dication also possesses radical character, since the absorption spectra in the potential range 0.4−0.8 V are characteristic for TTF radical cations. By further increasing the potential, the second couple of oxidation processes starts to occur, the most significant change in the optical spectra being the disappearance of the low-energy band together with the blue shift of the high-energy band toward λ_{max} = 428 nm. The apparent lack of differences between the absorption spectra of the tri- and tetracation is quite surprising, when considering the likely radical nature of the trication and the singlet ground state of the tetracation, by analogy with a TTF^{2+}. No absorption band was observed beyond 850 nm at any potential, thus ruling out the occurrence of intermolecular π-dimers. Moreover, neither concentration nor scan rate dependence of the spectra was detected.

Cyclic voltammetry measurements for the compounds **2**−**4** reveal first that the transformation in the λ^5-P derivative or complexation does not perturb the electron donor properties of the TTF moieties. Indeed, the oxidation potentials are only slightly shifted toward more anodic values (Supporting Information). Moreover, only splitting of the two first oxidation processes is now observed, with ΔE values of

(17) (a) Torrance, J. B.; Scott, B. A.; Welber, B.; Kaufman, F. B.; Seiden, P. E. *Phys. Rev. B* **1979**, *19*, 730. (b) Huchet, L.; Akoudad, S.; Levillain, E.; Roncali, J.; Emge, A.; Bäuerle, P. *J. Phys. Chem. B* **1998**, *102*, 7776.

(18) Pou-AméRigo, R.; Ortí, E.; Merchán, M.; Rubio, M.; Viruela, P. M. *J. Phys. Chem. A* **2002**, *106*, 631.

(19) Khodorkovsky, V.; Shapiro, L.; Krief, P.; Shames, A.; Mabon, G.; Gorgues, A.; Giffard, M. *Chem. Commun.* **2001**, 2736.

90 mV for **2** and 105 mV in the case of **3** and **4**. Subsequent oxidation into 3+ and 4+ species is accompanied by adsorption phenomena, which probably hinder the observation of wave splitting.

EPR Measurements. In order to investigate the electron delocalization in *cis*-**1** radical cation and dication species, which are electrochemically available at rather low oxidation potentials, we have performed solution EPR measurements coupled with electrochemistry. Note that the EPR technique allowed us to undoubtedly prove the full electron delocalization in the case of the radical cations of silicon- and germanium-bridged bis(TTFs) $(XMe_2)_2(o\text{-DMTTF})_2$ (X = Si, Ge).[12]

The hyperfine structure observed after oxidation of *cis*-**1** (Figure 7) is clearly consistent with the central part of a spectrum exhibiting a coupling of 0.48 G with 12 magnetically equivalent protons. Indeed, even though only 11 of the 13 expected lines are observed, the intensity distribution follows accurately that of the simulated spectrum (Supporting Information). As confirmation of this analysis, a single hyperfine coupling constant ($A_{iso} = 1.32$ MHz) is detected on the ^{1}H ENDOR spectrum (inset Figure 7). We can therefore confidently assign the hyperfine structure to the coupling with four methyl groups. Moreover, the corresponding isotropic constant amounts to half the value of the one measured on the radical cation of $(o\text{-DMTTF})(PPh_2)_2$ diphosphine, containing only two Me groups,[20] and it compares very well with that of 0.42 G observed in the case of $[(XMe)_2(o\text{-DMTTF})_2]^{+\bullet}$ (X = Si, Ge).[12] This clearly demonstrates that in $[cis\text{-}\mathbf{1}]^{+\bullet}$ the unpaired electron is delocalized over both TTF units, and hence a genuine intramolecular mixed valence state is generated, with each TTF bearing a $\delta = +0.5$ mean charge. Note that, as also observed in the case of the diphosphine $(o\text{-DMTTF})(PPh_2)_2$, no feature of the hyperfine structure is due to a coupling with the phosphorus atoms, a likely proof that no spin density is present on these P atoms. The same EPR spectrum is observed when the oxidation is carried out chemically, with 1 equiv of $NOBF_4$.

Further oxidation at higher potentials, or with 2 equiv of chemical oxidant, such as to generate the dication of *cis*-**1**, provokes a drastic modification of the spectrum: strong additional lines are observed leading to a rather complex spectrum (Supporting Information), which could not be reasonably simulated. In frozen solution, no half-field signal, characteristic for triplet species, could be detected, yet this is not surprising when considering the delocalized nature of our radicals. However, it is likely that no decomposition occurs since this new spectrum shows reversibility to the previous one, of $[cis\text{-}\mathbf{1}]^{+\bullet}$, upon lowering the potential, thus demonstrating once again the radical nature of the $[cis\text{-}\mathbf{1}]^{2+}$ species.

Since among the derivatives **2**−**4**, only the tungsten-based bimetallic complex **4** could be separated as *cis* and *trans* isomers by column chromatography, we have performed EPR investigations on *cis*-**4**. The spectrum of $[cis\text{-}\mathbf{4}]^{+\bullet}$ (Figure 8), electrochemically generated in a CH_2Cl_2 solution, appears to be more complex than that of the free ligand. The spectrum of such a large and fluxional radical ion is difficult to simulate since the shape of the lines is likely sensitive to internal motions. Moreover, as a consequence of the presence of metallic centers, the *g*-value (2.010) is appreciably larger than for the free ligand; the probable small anisotropy of the *g*-tensor is expected to also contribute to the complexity of the spectrum of this slowly tumbling radical. An acceptable simulation could nevertheless be obtained by considering an isotropic coupling of 0.62 G with 12 equivalent protons and a coupling of 0.37 G with two equivalent ^{31}P nuclei.

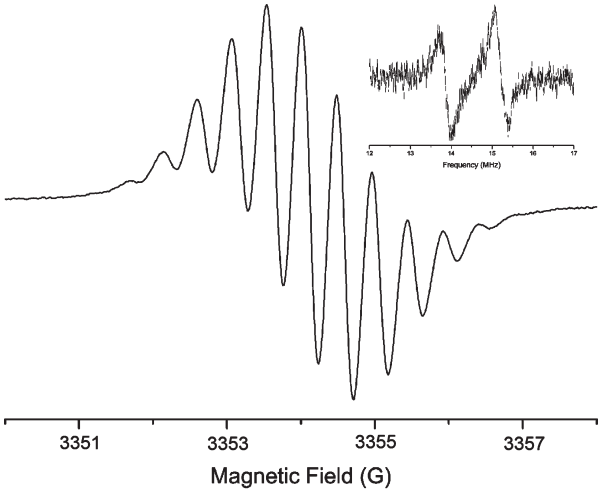

Figure 7. EPR spectrum of $[cis\text{-}\mathbf{1}]^{+\bullet}$ (CH_2Cl_2 sol., $(TBA)PF_6$ 0.2 M, $E = +0.4$ V vs Ag, $T = 300$ K, $\nu = 9426$ MHz,); $g_{iso} = 2.008$, $A_{iso} = 0.48$ G. Inset: ENDOR ^{1}H of *cis*-**1** oxidized by 1 equiv of $NOBF_4$ in CH_2Cl_2; $T = 270$ K, $\nu = 9593$ MHz, $A_{iso} = 1.32$ MHz.

It is clear that the functionalization at the P atoms induces some changes in the spin distribution in the radical species of **2**−**4** with respect to that in the oxidized ligand $[\mathbf{1}]^{+\bullet}$; yet it is very likely that full delocalization occurs in all the cases.

Theoretical Calculations. In order to have a deeper understanding of the electronic structures and to rationalize the EPR results, we have performed unrestricted DFT calculations with the Gaussian03 package[21] by using the B3LYP functional[22,23] and the 6-31+G* basis set for both the geometry optimization and the prediction of the electronic properties of $(cis\text{-}\mathbf{1})^{+\bullet}$. For the sake of comparison, calculations have also been carried out using other functionals and basis sets (see Experimental Section); the resulting values are reported in the Supporting Information.

In contrast with the crystal structure of neutral *cis*-**1**, which indicates a boat-type conformation of the central

(20) Gouverd, C.; Biaso, F.; Cataldo, L.; Berclaz, T.; Geoffroy, M.; Levillain, E.; Avarvari, N.; Fourmigué, M.; Sauvage, F. X.; Wartelle, C. *Phys. Chem. Chem. Phys.* **2005**, *7*, 85.

(21) Frisch, M. J.; Trucks, G. W.; Schlegel, H. B.; Scuseria, G. E.; Robb, M. A.; Cheeseman, J. R.; Montgomery, J. A., Jr.; Vreven, T.; Kudin, K. N.; Burant, J. C.; Millam, J. M.; Iyengar, S. S.; Tomasi, J.; Barone, V.; Mennucci, B.; Cossi, M.; Scalmani, G.; Rega, N.; Petersson, G. A.; Nakatsuji, H.; Hada, M.; Ehara, M.; Toyota, K.; Fukuda, R.; Hasegawa, J.; Ishida, M.; Nakajima, T.; Honda, Y.; Kitao, O.; Nakai, H.; Klene, M.; Li, X.; Knox, J. E.; Hratchian, H. P.; Cross, J. B.; Adamo, C.; Jaramillo, J.; Gomperts, R.; Stratmann, R. E.; Yazyev, O.; Austin, A. J.; Cammi, R.; Pomelli, C.; Ochterski, J. W.; Ayala, P. Y.; Morokuma, K.; Voth, G. A.; Salvador, P.; Dannenberg, J. J.; Zakrzewski, V. G.; Dapprich, S.; Daniels, A. D.; Strain, M. C.; Farkas, O.; Malick, D. K.; Rabuck, A. D.; Raghavachari, K.; Foresman, J. B.; Ortiz, J. V.; Cui, Q.; Baboul, A. G.; Clifford, S.; Cioslowski, J.; Stefanov, B. B.; Liu, G.; Liashenko, A.; Piskorz, P.; Komaromi, I.; Martin, R. L.; Fox, D. J.; Keith, T.; Al-Laham, M. A.; Peng, C. Y.; Nanayakkara, A.; Challacombe, M.; Gill, P. M. W.; Johnson, B.; Chen, W.; Wong, M. W.; Gonzalez, C.; Pople, J. A. *Gaussian 03, Revision B.03*; Gaussian, Inc.: Pittsburgh, PA, 2003.

(22) Becke, A. D. *J. Chem. Phys.* **1993**, *98*, 6548.

(23) Lee, C.; Yang, W.; Parr, R. G. *Phys. Rev. B* **1988**, *37*, 785.

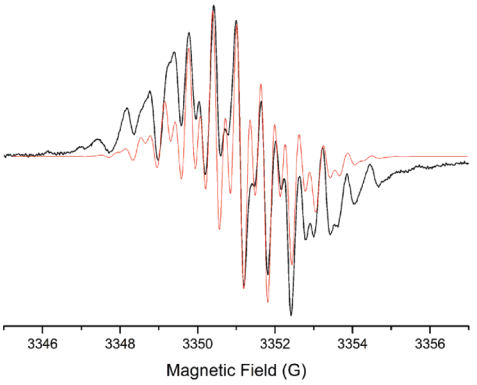

Figure 8. Experimental (black) and simulated (red) EPR spectra of $[cis\text{-}\mathbf{4}]^{+\bullet}$ (CH_2Cl_2 sol., (TBA)PF_6 0.2 M, $E = +0.45$ V vs Ag, $T = 300$ K, $\nu = 9426$ MHz); $g_{iso} = 2.010$, $A_{iso}(^1H_{Me}) = 0.62$ G, $A_{iso}(^{31}P) = 0.37$ G.

dihydrodiphosphine ring (dihedral angle $C_{TTF1}PPC_{TTF2} = -154.2°$), a previous optimization of this molecule[13] had led to a local minimum (*Min 1*, point group C_1) characterized by an almost planar conformation of the central ring (dihedral angle CPPC $= -177.1°$). New optimization of this molecule shows, however, that a second energy minimum (*Min 2*, point group C_2) is present. This energy minimum, *Min 2*, is hardly more stable than *Min 1* (-0.75 kcal·mol^{-1}); in the corresponding structure the central ring adopts a boat conformation and is strongly folded along the P···P hinge (dihedral angle CPPC $= -138.3°$) (Supporting Information). The presence of these three structures for *cis*-**1** suggests that exchange processes likely occur in solution.

Geometry optimization of the radical monocation $[cis\text{-}\mathbf{1}]^{+\bullet}$ affords an equilibrium geometry characterized by a distorted central six-membered ring within a boat-type conformation, with a folding angle along the P···P hinge of $-135.9°$ and planar TTF fragments directed toward the phenyl rings (Figure 9 and Supporting Information). The singly occupied orbital (SOMO), delocalized on the two redox-active units, with negligible contribution of P atoms, consists of the antisymmetrical combination of TTF π orbitals (Figure 9), while the SOMO-1 corresponds to the symmetrical combination of these orbitals.

The calculated isotropic hyperfine coupling constant with the lateral methyl protons amounts to 0.47 G, in agreement with the experimental value of 0.48 G (*vide supra*). The predicted $^{31}P-A_{iso}$ values are equal to -1.27 G, while no coupling with phosphorus is observed on the spectrum. This discrepancy is likely caused by the well-known difficulty to accurately predict the Fermi contact interaction with ^{31}P nuclei.[24,25] The calculation of $^{31}P-A_{iso}$ is especially *critical* for $\mathbf{1}^{+\bullet}$ since for this radical there is no contribution of the phosphorus orbitals to the SOMO and the ^{31}P isotropic coupling results only from spin polarization. Related to this difficulty, the predicted couplings show some dependence upon the functional and basis sets used for the calculations (Supporting Information): for example at the BLYP/6-31G* level the ^1H and ^{31}P couplings are equal to 0.6 and -0.8 G, respectively. Another cause for the slight difference between experimental and calculated ^{31}P coupling constants probably lies in the vibrational effects. There are 174 vibration modes for $\mathbf{1}^{+\bullet}$, and we have calculated the effect of some of these modes on the ^{31}P coupling constants by following the method of Barone.[26] It is found that most of these modes do not affect the $^{31}P-A_{iso}$ values; for some of them, however, a slight decrease of the coupling is indeed calculated. This is the case, for example, for the vibration at 1435 cm^{-1}, corresponding to an antisymmetrical combination of stretching of the TTF double bonds, which leads to a decrease of 0.10 G of the absolute value of $^{31}P-A_{iso}$. An exhaustive investigation of all vibrations for such a large system is beyond the scope of this work. It seems nevertheless reasonable to admit that the real ^{31}P hyperfine splitting is very close to zero. Moreover, it should be remarked that in the radical cation of (*o*-DMTTF)-$(PPh_2)_2$[20] the calculated isotropic hyperfine coupling with the phosphorus atoms is only 0.14 G, and hence not experimentally observed, which is indicative of the variation of this constant with the mutual orientation of the TTF and phosphino groups.

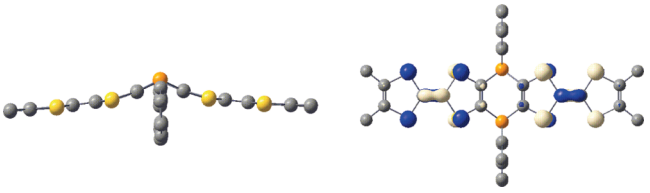

Figure 9. Optimized geometry of $[cis\text{-}\mathbf{1}]^{+\bullet}$ (left) and SOMO (right).

Furthermore, we have undertaken a theoretical study on the dication $[cis\text{-}\mathbf{1}]^{2+}$ species, with the aim to estimate the relative stability of the triplet and singlet states. Accordingly, the calculations afford a triplet state that is more stable than the singlet one by 11.7 kcal mol^{-1}, with an overall equilibrium geometry quite similar to that of the radical cation, i.e., boat conformation of the central ring (folding angle $-129.1°$) and planarity of the TTF units (Supporting Information). These theoretical results are in agreement with a full delocalization of the electron in the radical monocation and with the radical character of the dication, as suggested by the UV−vis and EPR spectroelectrochemistry measurements (*vide supra*).

Conclusions

In this study we have demonstrated first the versatility of the redox-active bis(TTF)-1,4-dihydro-1,4-diphosphinine **1**, affording λ^5-P derivatives or bimetallic complexes. Single-crystal X-ray structures of some of these compounds undoubtedly prove their *cis* or *trans* stereochemistry and demonstrate a certain flexibility of the central six-membered ring, together with various supramolecular architectures characterized by short intermolecular contacts, an important prerequisite in view of preparing radical cation salts or charge transfer complexes possessing conducting and/or magnetic properties. UV−vis spectroelectrochemistry measurements on the *cis*-**1** isomer allowed us to detect the optical signature of the oxidized species up to the tetracation. EPR investigations on the same compound, coupled with theoretical calculations at the DFT level, definitely prove the electron delocalization over both TTF

(24) Nguyen, M. T.; Creve, S.; Eriksson, L. A.; Vanquickenborne, L. G. *Mol. Phys.* **1997**, *91*, 537.
(25) Barone, V.; Cimino, P.; Stendardo, E. *J. Chem. Theory Comput.* **2008**, *4*, 751.
(26) Barone, V.; Grand, A.; Minichino, C.; Subra, R. *J. Chem. Phys.* **1993**, *99*, 6787.

units in the radical cation $[cis\text{-}\mathbf{1}]^{+\bullet}$ and the radical nature of the dication $[cis\text{-}\mathbf{1}]^{2+}$, for which the most stable ground state is the triplet. EPR measurements demonstrate also the electron delocalization in the bimetallic W-based complex $[cis\text{-}\mathbf{4}]^{+\bullet}$. Current investigations in our groups deal with the preparation of radical cation salts derived from these new functional donors and also with the coordination chemistry of the redox-active ligand **1** with various metallic fragments, possibly endowed with magnetic or optical properties.

Experimental Section

General Procedures. Reactions were carried out under nitrogen, THF was distilled from Na/benzophenone, and (THF)M(CO)$_5$ (M = Mo, W) was freshly prepared by irradiation of M(CO)$_6$ solutions in THF. A Stahler TNN 15/32 lamp was used, with $\lambda = 254$ nm and power consumption of 15 W. NMR spectra were recorded on a Bruker Avance DRX 500 spectrometer operating at 500.04 MHz for ^{1}H, 125.75 MHz for ^{13}C, and 202.39 MHz for ^{31}P. Chemical shifts are expressed in parts per million (ppm) downfield from external TMS. The following abbreviation is used: s, singlet (NMR) or strong (IR). Elemental analyses were performed by the "Service d'Analyse du CNRS" at Gif/Yvette, France. Compound **1** was synthesized according to the published procedure.[13]

Synthesis of (PhPS)$_2$(*o*-DMTTF)$_2$ (2). A large excess of sulfur (360 mg, 11.2 mmol) was added to a solution of **1** (97 mg, 0.14 mmol) in THF (50 mL). The mixture was heated under reflux until the disappearance of the ^{31}P NMR signal of the starting material (about 24 h). The solvents were then evaporated, and the resulting solid was washed several times with pentane. After chromatographic purification on a silica gel column with methylene chloride/cyclohexane (1:1) as eluent, a mixture of *cis*-**2**/*trans*-**2** (1.5:1) was obtained as an orange solid (80 mg, 72%). Crystals of *trans*-**2**, suitable for X-ray crystallographic studies, were obtained upon evaporation of a methylene chloride solution. ^{31}P NMR (THF): δ 11.6 (s, *cis*), 12 (s, *trans*). Anal. Calcd for $C_{28}H_{22}P_2S_{10}$: C, 45.37; H, 2.99. Found: C, 45.59; H, 2.85.

Synthesis of [(PhP)Mo(CO)$_5$]$_2$(*o*-DMTTF)$_2$ (3). A solution of (THF)Mo(CO)$_5$ (38 mL), obtained by UV irradiation for 55 min of Mo(CO)$_6$ (2.64 g, 10 mmol) in THF (300 mL), was added to **1** (84 mg, 0.12 mmol) in THF (10 mL), and the mixture thus obtained was heated at 50 °C for 8 h. After evaporation of solvents, the crude product was purified by column chromatography with silica gel (cyclohexane/toluene, 1:1) to afford **3** as a brown solid (*cis*/*trans* 3:1) (70 mg, 49%). Different types of crystals for the two isomers were obtained in toluene at low temperature, and the mechanical separation of the isomers was possible. Indeed, *cis*-**3** crystallized as thin needles, while *trans*-**3** crystallized as prisms. Only the crystals of *trans*-**3** were suitable for X-ray crystallographic studies. ^{31}P NMR (THF): δ 18.9 (s; *cis*), 20 (s, *trans*). IR (cm^{-1}, KBr): 2077 s (CO), 2032 s (CO), 1954 s (CO). Anal. Calcd for $C_{38}H_{22}Mo_2O_{10}P_2S_8$: C, 39.72; H, 1.93. Found: C, 39.58; H, 1.81.

Synthesis of [(PhP)W(CO)$_5$]$_2$(*o*-DMTTF)$_2$ (4). **1** (0.1 g, 0.15 mmol) was stirred with an excess of (THF)W(CO)$_5$, obtained by UV irradiation for 65 min of W(CO)$_6$ (3.52 g, 10 mmol) in THF (300 mL), at 50 °C during 4 h in THF. The resulting isomeric bimetallic complexes (*cis*/*trans* 6:1) were separated by column chromatography with a hexane/toluene (60:40) mixture, eluting first the *trans*, then the *cis* isomer. Overall yield: 0.18 g (92%). The *trans* isomer was recrystallized from toluene, whereas the *cis* one was crystallized by slow diffusion of pentane into a CH_2Cl_2 solution. ^{31}P NMR (THF): δ 0.9 (s, *cis*), 0.4 (s, *trans*). IR (cm^{-1}, KBr): 2078 s (CO), 2034 s (CO), 1928 s (CO). Anal. Calcd for $C_{38}H_{22}O_{10}P_2S_8W_2$: C, 34.45; H, 1.68. Found: C, 34.24; H, 1.54.

X-ray Structure Determinations. Details about data collection and solution refinement are given in Table 2. X-ray diffraction measurements were performed on a Bruker Kappa CCD diffractometer for *trans*-**2** and *trans*-**3** and on a Stoe Imaging Plate System for *cis*-**4** and *trans*-**4**, both operating with a Mo Kα (λ = 0.71073 Å) X-ray tube with a graphite monochromator. The structures were solved (SHELXS-97) by direct methods and refined (SHELXL-97) by full-matrix least-squares procedures on F^2.[27] All non-H atoms of the donor molecules were refined anisotropically, and hydrogen atoms were introduced at calculated positions (riding model), included in structure factor calculations but not refined. For the structure *trans*-**3** the carbon atoms of the disordered toluene molecule were refined isotropically, while the corresponding hydrogen atoms were not introduced. In the structure of *cis*-**4** the methylene chloride molecule is also highly disordered; therefore the carbon atom could not be assigned. Finally, in the structure of *trans*-**4** the crystallization toluene molecule was not disordered; therefore the carbon atoms were refined anisotropically, and hydrogen atoms were introduced at calculated positions (riding model), included in structure factor calculations but not refined. Crystallographic data for the structures have been deposited in the Cambridge Crystallographic Data Centre, deposition numbers CCDC 720073 (*trans*-**2**), CCDC 720074 (*trans*-**3**), CCDC 239192 (*cis*-**4**), and CCDC 239191 (*trans*-**4**). The quality of the crystals of *cis*-**3** (thin needles) was not sufficient for an accurate determination of its structure; however the cell parameters could be determined as follows: *cis*-**3**, red thin needles, triclinic system, $a = 8.694(10)$ Å, $b = 24.416(198)$ Å, $c = 26.493(86)$ Å, $\alpha = 63.24(11)°$, $\beta = 89.88(16)°$, $\gamma = 89.42(24)°$, $V = 5021.16$ Å^3.

Electrochemical Studies. Cyclic voltammetry measurements were performed using a three-electrode cell equipped with a platinum millielectrode of 0.126 cm^2 area, a silver wire pseudoreference electrode, and a platinum wire counter electrode. The potential values were then readjusted with respect to the saturated calomel electrode (SCE), using ferrocene as internal reference. The electrolytic media involved a 0.1 mol·L^{-1} solution of (n-Bu$_4$N)PF$_6$ in CH_2Cl_2. All experiments have been performed at room temperature at 0.1 V·s^{-1}. Experiments have been carried out with an EGG PAR 273A potentiostat with positive feedback compensation.

Spectroelectrochemistry. Spectroelectrochemical experiments on *cis*-**1** were performed in a cell made of Teflon, in thin-layer cyclic voltammetry (TLCV) conditions.[28] The number of the electrons involved in the redox processes has been precisely determined by the use of dichloronaphtoquinone as internal standard. A 2 mm diameter stationary Pt disk was used as the working electrode and a Pt wire as counter electrode. A Lambda 19 Perkin-Elmer spectrophotometer was employed. The current was provided by an EGG PAR 273A potentiostat; a scan rate of 1.25 mV s^{-1} was used. HPLC-grade methylene chloride was used as solvent and (n-Bu$_4$N)PF$_6$ (0.4 M) as supporting electrolyte.

EPR Measurements. EPR and ENDOR spectra were recorded on a Bruker ESP 300 spectrometer (X-band) equipped with a variable-temperature attachment B-VT-2000. Electrochemical oxidations at a controlled potential were performed by using a homemade electrolytic cell. This quartz cell, similar to the cell described by Fernando et al.,[29] contains a silver wire as a pseudo reference electrode; the working and counter electrodes are in platinum. This cell can be positioned inside the variable-temperature insert and allows measurement of EPR spectra at a controlled voltage over a wide range of temperatures. All measurements are carried out under a nitrogen atmosphere with

(27) Sheldrick, G. M. *Programs for the Refinement of Crystal Structures*; University of Göttingen: Göttingen, Germany, 1996.
(28) Gaillard, F.; Levillain, E. *J. Electroanal. Chem.* **1995**, *398*, 77.
(29) Fernando, K. R.; McQuillan, A. J.; Peake, B. M.; Wells, J. *J. Magn. Reson.* **1986**, *68*, 551.

rigorously degassed solutions. Chemical oxidations were performed under a nitrogen atmosphere in a glovebox.

Computational Details. Geometry optimization as well as hyperfine coupling calculations were performed with the Gaussian03 package[21] using the B3LYP functional[22,23] and the 6-31+G* basis sets. Minima were characterized with harmonic frequency calculations (no imaginary frequencies). As reported in the Supporting Information, additional single-point calculations were also run at the optimized geometry using different functionals (LDA, BP86, BLYP, PBEPBE, PW91PW91, B1LYP) and basis set functions (6-31G*, aug-cc-pVDZ, N07D). In another set of calculations, the geometry of the radical monocation was optimized with the Turbomole package[30] (B-P86 functional and SV(P) standard basis set), and the properties were calculated with the B3LYP functional and the TZVP basis set (Supporting Information). Molecular orbitals were represented by using the GaussView program.[31]

(30) Ahlrichs, R.; Bär, M.; Häser, M.; Horn, H.; Kölmel, C. *Chem. Phys. Lett.* **1989**, *162*, 165.
(31) *GaussView 3.0*; Gaussian Inc.: Pittsburgh, PA.

Acknowledgment. Financial support from the Ministry of Education and Research (grant to I.D.) and the French Ministry of Foreign Affairs through a Germaine de Staël 2006−2007 (PAI 10613RJ) project is gratefully acknowledged. This work was also supported by the CNRS (France) and the Swiss National Science Foundation (Switzerland).

Supporting Information Available: X-ray crystallographic data for *trans*-**2**, *trans*-**3**, *cis*-**4**, and *trans*-**4** in CIF format and additional structural figures with bond distances and angles; cyclic voltammetry curves; EPR details and figures; and theoretical calculation details. This material is available free of charge via the Internet at http://pubs.acs.org.